Journal of Translational Medicine

RESEARCH

Open Access

STK40 inhibits trophoblast fusion by mediating COP1 ubiquitination to degrade P57^{Kip2}

Xia Li[1,2†], Li-Zhen Shao[1,2†], Zhuo-Hang Li[2,3], Yong-Heng Wang[1,2], Qin-Yu Cai[1,2], Shun Wang[1], Hong Chen[1,2], Jie Sheng[1,2], Xin Luo[2,4], Xue-Mei Chen[2], Ying-Xiong Wang[1*], Yu-Bin Ding[2*] and Tai-Hang Liu[1,2*]

Abstract

Background The syncytiotrophoblast (SCT) layer in the placenta serves as a crucial physical barrier separating maternal-fetal circulation, facilitating essential signal and substance exchange between the mother and fetus. Any abnormalities in its formation or function can result in various maternal syndromes, such as preeclampsia. The transition of proliferative villous cytotrophoblasts (VCT) from the mitotic cell cycle to the G0 phase is a prerequisite for VCT differentiation and their fusion into SCT. The imprinting gene P57^{Kip2}, specifically expressed in intermediate VCT capable of fusion, plays a pivotal role in driving this key event. Moreover, aberrant expression of P57^{Kip2} has been linked to pathological placental conditions and adverse fetal outcomes.

Methods Validation of STK40 interaction with P57^{Kip2} using rigid molecular simulation docking and co-immunoprecipitation. STK40 expression was modulated by lentivirus in BeWo cells, and the effect of STK40 on trophoblast fusion was assessed by real-time quantitative PCR, western blot, immunofluorescence, and cell viability and proliferation assays. Co-immunoprecipitation, transcriptome sequencing, and western blot were used to determine the potential mechanisms by which STK40 regulates P57^{Kip2}.

Results In this study, STK40 has been identified as a novel interacting protein with P57^{Kip2}, and its expression is down-regulated during the fusion process of trophoblast cells. Overexpressing STK40 inhibited cell fusion in BeWo cells while stimulating mitotic cell cycle activity. Further experiments indicated that this effect is attributed to its specific binding to the CDK-binding and the Cyclin-binding domains of P57^{Kip2}, mediating the E3 ubiquitin ligase COP1-mediated ubiquitination and degradation of P57^{Kip2}. Moreover, abnormally high expression of STK40 might significantly contribute to the occurrence of preeclampsia.

†X. Li and L.Z. Shao contributed equally to this work.

*Correspondence:
Ying-Xiong Wang
yxwang@cqmu.edu.cn
Yu-Bin Ding
dingyb@cqmu.edu.cn
Tai-Hang Liu
liuth@cqmu.edu.cn

Full list of author information is available at the end of the article

Conclusions This study offers new insights into the role of STK40 in regulating the protein-level homeostasis of $P57^{Kip2}$ during placental development.

Keywords $P57^{Kip2}$, STK40, Placenta, Trophoblast, Cell fusion, Preeclampsia

Background

The placenta stands as a crucial cornerstone for maintaining a successful pregnancy and ensuring healthy fetal development. It serves the mission of nutrition transmission, gas exchange, immune tolerance, and secretion of pregnancy-specific hormones [1]. Throughout pregnancy, mononuclear placental villous cytotrophoblast (VCT) continually proliferate and fuse into syncytiotrophoblast (SCT), eventually forming a semi-permeable barrier epithelium covering the surface of placental villi, which is the main place for material exchange and hormone secretion between mother and fetus. Number of studies have demonstrated that the formation or function defects of SCT can lead to various placental-derived diseases, such as preeclampsia (PE), premature delivery, fetal growth restriction (FGR), and even stillbirth [2, 3]. As ongoing debates continue regarding whether abnormalities in trophoblast cells are the cause or a consequence of these diseases, it remains crucial to conduct comprehensive investigations into the key steps and factors regulating the proliferation and differentiation of trophoblast cells to address this issue. This will also aid in identifying effective intervention targets for clinical treatment.

The differentiation and fusion of VCT into SCT involved complex interactions among multiple signaling pathways, epigenetic modification, transcription factors, cytoskeletal proteins, and plasma membrane components [4]. The cell cycle plays a crucial role in balancing the self-renewal and differentiation of VCT. Cells in the growth phase exit the cell cycle and enter a state commonly referred to as the 'resting' or 'quiescent' phase (G0 phase). The single-cell RNA sequencing (RNA-seq) analysis and experiments have clarified that the exit of VCT from the mitotic cell cycle to form intermediate cells with fusion competence in the G0 phase is a prerequisite for their subsequent fusion [5]. While premature exit from the mitotic cell cycle is necessary for the up-regulation of the classical fusion-driving factor Syncytin-2, forcibly expressing Syncytin-2 in proliferating VCT can induce physical cell fusion; however, this process leads to instability and dysfunctionality of SCT [6]. Moreover, the high expression of transcriptional coactivator YAP upregulates stem cell and cell cycle-related genes, promoting self-renewal of VCT while inhibiting their fusion [7]. The role of classical cell cycle inhibitors such as $P57^{Kip2}$, $P21^{Cip1}$, and $P27^{Kip1}$ in regulating the cell cycle and differentiation of VCT has consistently been a focal point of attention [8]. Among them, the paternally imprinted gene $P57^{Kip2}$ (hereinafter referred to as P57), encoded by CDKN1C, is the least studied member of the family. It was found to be highly expressed in embryos and downregulated with age-dependent and ultimately expressed only in specific tissues like the adult placenta, brain, skeletal muscle, and lung. Abnormal low expression or loss of P57 expression is associated with the proliferation of pathological trophoblast cells. Mutations or abnormal expression of P57 can lead to excessive cell proliferation, resulting in the development of hydatidiform mole. Currently, P57 serves as a key indicator used for clinical diagnosis and classification of hydatidiform mole [9, 10].

Our prior research, along with that of Takahashi et al., has concurrently discovered that high expression of P57 inhibited VCT proliferation and promoted the fusion of VCT, and elevated levels of P57 drive the generation of intermediate VCT [11, 12]. Moreover, gene knockout technology has demonstrated that the absence of P57 expression in pregnant mice could induce PE-like symptoms [13]. More importantly, the proportion of P57-positive intermediate VCT was significantly lower in early-onset PE placenta compared to normal human placenta [14]. Combined with the phenotype of excessive immature proliferative VCT and damaged SCT in the placenta of PE patients [3], it can be speculated that PE placenta experienced abnormal cell cycle regulation due to the withdrawal of VCT from mitosis, resulting in impaired VCT fusion and placental development and dysfunction in PE placenta. Therefore, abnormal expression of P57 in the placenta may be one of the key factors contributing to the imbalance between VCT proliferation and differentiation, resulting in impaired syncytialization and ultimately inducing PE.

To delve deeper into the regulatory mechanism of P57 in VCT fusion, immunoprecipitation-mass spectrometry analysis was employed to identify the potential interaction protein of P57, and a new interacting protein STK40 of P57 was verified. Then, through a variety of VCT fusion models and experiments, the interaction sites and regulatory mechanisms between STK40 and P57 and their roles in physiology and pathology were revealed. This study has laid a theoretical foundation for comprehending the pathological mechanism underlying the imbalance in VCT proliferation and differentiation, mediated by abnormal cell cycle regulation, which is implicated in the occurrence of PE.

Materials and methods

Human placental tissue collection and isolation of primary human trophoblast cell

All placentas were voluntarily donated by patients at the First Affiliated Hospital of Chongqing Medical University with informed consent and institutional approval. The Human Research Ethics Board of the Chongqing Medical University approved the human placental tissues collection procedures (#2,022,127). Placental tissues were collected from normal pregnant women with voluntary termination of pregnancy ($n=3$, gestational age 6–8 weeks), those with PE ($n=6$, gestational age 36–38 weeks), and age-matched normal controls ($n=6$, gestational age 38–40 weeks). The diagnostic criteria for PE patients refer to the American College of Obstetrics and Gynecology (ACOG) guideline that new-onset hypertension (systolic blood pressure ≥ 140 mmHg and/or diastolic blood pressure ≥ 90 mmHg; average of two measurements) after 20 weeks of gestation with proteinuria or other organ damage [15]. The exclusion criteria included women with other systemic diseases, such as preexisting hypertension, cardiovascular diseases, renal disease, immune disease, or other gestational complications. To isolate primary human trophoblast cells (PHT), normal term placenta was washed twice with normal saline, cut into small pieces using sterile scissors, and then digested with an enzyme mixture containing trypsin (Sigma-Aldrich, St. Louis, MO, USA), DNase (Roche, Basel, Switzerland), and Dispase (Sigma-Aldrich). Percoll (GE Healthcare, Chicago, IL, USA) gradient centrifugation was utilized to enrich VCT, and the collected cells were cultured in DMEM medium (Sigma-Aldrich) supplemented with 10% fetal bovine serum (FBS, Gibco, Waltham, MA, USA). VCT cells spontaneously fused into SCT cells in 48 h of culture in vitro, so VCT cells and SCT cells were collected separately after 3 h and 48 h of culture.

Cell culture

BeWo cells (American Type Culture Collection, ATCC, Manassas, VA, USA) were cultured in F12K medium (ATCC) supplemented with 10% FBS. To induce cell fusion, BeWo cells were treated with 25 μM forskolin (FSK, Sigma-Aldrich) for 48–72 h. HEK-293T (Cell Bank, Chinese Academy of Sciences) was cultured in DMEM (Gibco) supplemented with 10% FBS. All cells were cultured in 37 °C, 5% CO_2 incubator. Prior to use, all cell lines were tested negative for mycoplasma contamination using a mycoplasma detection kit (TransGen Biotech, Beijing, China).

Mass spectrometry

Human placental villi from early pregnancy were collected and then lysed on ice for 20 min in 1 ml of RIPA buffer (Beyotime, Shanghai, China) supplemented with 1 × Phenylmethanesulfonyl fluoride (PMSF, Beyotime). Whole cell lysates were subjected to immunoprecipitation (IP) overnight at 4 °C using P57 antibody (Cell Signaling Technology, Danvers, MA, USA; catalog: #2557S) or normal rabbit IgG (Cell Signaling Technology, Danvers, MA, USA; catalog: #2729). The 25 μl prewashed Protein A/G magnetic beads (Thermo Scientific Pierce, Waltham, MA, USA; catalog: 88,802) were added to the lysis buffer and antibody mixture and incubated at room temperature for one hour. IP protein was separated by SDT buffer (4% SDS, 100 mM Tris-HCL, 1 mM DTT, PH = 7.6). Peptide detection was performed by liquid chromatography-tandem mass spectrometry (LC-MS/MS) in Applied Protein Technology (Shanghai, China), and coupling analysis was performed with Easy NLC by Q Exactive mass spectrometer.

Plasmid construction

The plasmids utilized in this study were generated through following steps: the eukaryotic expression vector pCDH was first linearized by restriction endonuclease, ECoR-I (New England Biolabs, NEB, Beverly, MA, USA) and Not-I (NEB), and the linearized carriers were then recovered by agarose gel electrophoresis and using a gel recovery kit (Omega Bio-Tek, Norcross, GA, USA). Fragments comprising STK40 (Genbank id: NM_001282547.2), P57 (Genbank id NM_001122630.2), and ubiquitin (UB; Genbank id: X04803.2) were obtained from the human placental villus cDNA library and fused with HA or MYC tag, then cloned into pCDH vector using homologous recombination, respectively. All fragments were generated using high-fidelity polymerase (TransGen Biotech, China) and homologous recombination was performed by Exnase II ligase (Vazyme, Nanjing, China). Finally, the STK40 vector containing the HA tag, P57 truncated mutant containing MYC tag, and HA-tag Ub vector were obtained. The COP1 vector was purchased from Gene Copoeia (Guangzhou, China; Genbank id: NM_022457.7). Synthesized shRNA targeting STK40 (Genbank id: NM_032017.3, 5′-CCGGATGGTT AAGAAGATGAA-3′) was cloned into a pSIH1 vector to construct knockdown of STK40 vector.

Lentivirus packaging and infection

HEK-293T cells were cultured in 60 mm dishes until reaching 60–80% confluence. A mixture of psPAX2, pVSVG, the target plasmid, and polyethylenimine Linear transduction reagent (Polysciences Co., USA) was added to the cells. Lentiviral particles were collected 48–72 h after inoculation. The collected virus particles were used to infect BeWo cells after adding 2 μg/ml polybrene. After 12 h of infection, cells infected with pCDH or shRNA were selected with 6 μg/ml puromycin. The

selected cells were re-inoculated into a six-well plate containing F12K complete medium supplemented with 1 μg/ml puromycin and 10% FBS to continue culture to obtain stable overexpression or knockdown of STK40 cell lines.

Co-immunoprecipitation (Co-IP)

To extract protein, samples of human villus tissue or cells were lysed in a buffer containing protease and phosphatase inhibitors. The resulting mixture was centrifuged at 12,000 g for 15 min at 4 °C to obtain the supernatant containing the protein. Additionally, a tenth of the lysate was extracted as an input sample. The remaining lysates were divided into two equal parts. Subsequently, the target antibody and IgG were separately added to each part, followed by overnight incubation at 4 °C. Afterward, 25 μl prewashed Protein A/G magnetic beads were introduced to the lysate and antibody mixture, and the solution was incubated at room temperature for one hour. Proteins associated with Protein A/G beads were collected using a magnetic rack. The protein was eluted with SDS polyacrylamide gel electrophoresis (SDS-PAGE) washing buffer and subjected to Western blot (WB).

Immunofluorescence

Cells were seeded on a sterile glass slide and placed in a 24-well plate with or without FSK treatment. After incubation, the cells were gently washed three times with phosphate buffered saline (PBS), and fixed with 4% paraformaldehyde for 15 min. Following fixation, the cells underwent three additional washes with PBS and were permeabilized with a 0.1% Triton X-100 PBS solution for 15 min. To minimize non-specific binding, the cells were incubated in a PBS solution containing 3% bovine serum albumin (BSA) for an hour. Next, the primary antibody was added to the cells and allowed to incubate overnight at 4 °C. Details of antibodies were as follows: Vimentin (1:200, Bioss, Woburn, MA, USA; catalog: BS-0756R), Cytokeratin-7 (CK7, ZSbio, Beijing, China; catalog: ZM-007), STK40 (1:200, Biorbyt, Cambridge, United Kingdom; catalog: orb101780), E-Cadherin (E-CAD, 1:200, CST; catalog: #14,472). After three washes with PBS, the cells were stained with the corresponding goat anti-rabbit IgG (H+L) cross-adsorbed secondary antibody Alexa Fluor 488/goat anti-mouse IgG (H+L) cross-adsorbed secondary antibody Alexa Fluor 594 (1:1000; Thermo Fisher Scientific) and incubated for an hour. Finally, the cells were counterstained with DAPI (1:1000; Beyotime) to visualize the nucleus. Immunofluorescence (IF) signals were captured by using confocal laser scanning microscopy (CLSM) (Nikon, Tokyo, Japan).

Protein extraction and western blot

Whole cells were lysed in RIPA buffer (Beyotime) supplemented with 1 × PMSF, and the protein concentration was determined using the BCA protein assay kit (Beyotime). All protein imprinting was performed using a micro-electrophoresis system (Bio-Rad, Hercules, CA, USA). The total protein was separated on a 10% SDS-PAGE gel and transferred to a polyvinylidene fluoride (PVDF) membrane (Millipore, Burlington, MA, USA). Following blocking with 5% skim milk at room temperature for an hour, the membrane was incubated with primary antibodies overnight at 4 °C with the following primary antibodies: STK40 (1:1000, Invitrogen; catalog: PA5-22165), P57 (1:1000, Proteintech, Wuhan, China; catalog: 66794-1-Ig), CGβ (1:1000, Proteintech; catalog: 11615-1-AP), E-CAD (1:1000, CST; catalog: #14,472), GAPDH (1:1000, Beyotime; catalog: AF0006), Myc-Tag (1:1000, CST; catalog: #2276), COP1 (1:1000, Abcam, Cambridge, MA, USA; catalog: ab56400), Ubiquitin (1:1000, Abmart, Shanghai, China; catalog: T55965). Subsequently, the membrane was incubated with the corresponding Goat anti-Rabbit/Mouse IgG (H+L) Secondary Antibody, HRP (1:10000, Thermo Scientific Pierce, C31460100/C31430100) at 37 °C for one hour. The target protein was detected using the ECL-Plus kit (NCM Biotech, Suzhou, China).

RNA isolation, cDNA synthesis, and RT-qPCR

Total RNA was isolated using Trizol reagent (Takara, Shiga, Japan). RNA concentration was measured by spectrometer (Bio-rad). For the synthesis of cDNA, 0.1–0.5 μg of total RNA was used for reverse transcription according to the reverse transcription kit (TransGen Biotech, China). real-time quantitative PCR (RT-qPCR) was performed using SYBR Green qPCR Master Mix (TransGen Biotech, China) and real-time PCR system (Bio-Rad). Primer sequences used were as follows: STK40 forward, 5′-CAGCACTACGTCATCAAGGAG-3′, STK40 reverse, 5′-CGATGTGTCCTCTCTTGTTGAGC-3′; P57 forward, 5′-GCGGCGATCAAGAAGCTGT-3′, P57 reverse, 5′-GCTTGGCGAAGAAATCGGAGA-3′; and GAPDH forward, 5′-GGAGCGAGATCCCTCCAAAAT-3′, GAPDH reverse, 5′-GGCTGTTGTCATACTTCTCATGG-3′. GAPDH was used as a standardized internal control. The specificity of the fluorescence signal was verified by melting curve analysis and gel electrophoresis. The expression level of the target gene was determined by the $2^{-\Delta\Delta CT}$ method.

Cell viability and proliferation assays

Cell viability was measured by Cell Counting Kit 8 (CCK8, NCM Biotech). Cells were seeded into 96-well tissue culture plates at a density of 3×10^3 cells per well. At each time point, 10 μl of CCK8 solution was added to each well, and the plates were incubated at 37 °C for two hours. The absorbance at 450 nm was measured using a microplate reader (Molecular Devices, San Jose, CA,

USA). Cell proliferation was determined using 5-ethynyl-2′-deoxyuridine (EdU) assay. Briefly, cells were inoculated in cell crawls at a density of 1×10^4 cells and cultured overnight. The cells were then treated with 10 μM 5-Fu for 24 h. Next, 10 μM EdU (Beyotime) was added to the medium and incubated for an additional 12–24 h. Cells were fixed and stained according to the manufacturer's instructions.

Cell cycle assay

STK40-OE and sh-STK40 cells and their control cells were seeded in a six-well culture plate and cultured to 80% confluence. Cell cycle analysis was conducted via nuclear Propidium Iodide (PI, Beyotime) staining, and PI absorbance was measured by BD FACSCelesta Multicolor Flow Cytometer (BD Biosciences, San Jose, CA, USA).

Rigid molecular simulation docking

The PDB format files of the 3D crystal structures of P57 and STK40 proteins were obtained from the UniProt protein database (https://www.uniprot.org/). The model calculation was carried out using the GRAMM-X protein-protein docking server (https://gramm.compbio.ku.edu/), with P57 was selected as the receptor and STK40 as the ligand to analyze the two full-length protein groups. Docked complexes were analyzed using the PDBePISA server (https://www.ebi.ac.uk/msd-srv/prot_int/pistart.html). Results are visualized using PyMOL (Version 2.5.7).

RNA sequencing

Stably transfected cell lines, including STK40-OE and sh-STK40, as well as their respective control counterparts, were harvested, and total RNA was extracted using Trizol (Takara). RNA integrity was evaluated through 1.0% agarose gel electrophoresis. Subsequently, the RNA that meets the required standards was sent to Personalbio (Shanghai, China) for cDNA library preparation and RNA-seq. Samples were indexed and sequenced on an Illumina NovaSeq 6000. Raw reads were quality-controled and cleaned using FastQC (Version 0.11.9) and fastp (Version 0.23.1), and then aligned to the human genome GRCh38.p13 using HISAT2 (version 2.2.1). Gene counts were derived using Subread: featureCount (version 2.0.3). The DESeq2 package in R (Version 4.3.1) was used to analyze differentially expressed genes (DEGs) in RNA-seq data. Genes with a p-value <0.05 and an absolute fold change >0.5 were considered DEGs. Volcano plots show the expression patterns of these DEGs. Gene ontology (GO) and Kyoto Encyclopedia of Genes and Genomes (KEGG) pathway analysis were used to explore the possible functions of these DEGs.

Statistical analysis

Statistical analysis was performed using GraphPad Prism software (Version 5.0). Each experiment was repeated independently at least three times. Significant changes between the two groups were analyzed by Student's t-test. A value of $P<0.05$ was considered significant, denoted as * $P<0.05$, ** $P<0.01$, and *** $P<0.001$. All data are expressed as mean ± standard deviation (SD).

Results

1. STK40 is a novel interacting protein of P57

To delve into the regulatory mechanism of P57 during VCT fusion, the Co-IP experiments targeting P57 were performed using human villus tissue cells obtained from pregnancies at 6–8 weeks. Subsequently, protein mass spectrometry analysis was employed to identify the potential interacting proteins (IPs). A total of 118 IPs were finally identified (Supplementary Table S1), including well-known P57 IPs such as CCND1, CDK1, and CDK2, and various potential interacting proteins such as STK40, RAP1B, and NID2. GO analysis revealed that the biological process (BP) of the IPs were mainly enriched in the regulation of the G2/M transition of the mitotic cell cycle. Moreover, the cellular components (CC) of IPs were enriched in the cyclin-dependent protein kinase holoenzyme complex. The molecular function (MF) of the IPs showed enrichment in protein serine kinase activity (Fig. 1A). KEGG signaling pathway enrichment analysis confirmed that IPs were closely related to the p53 signaling pathway (Fig. 1B).

To further screen the high-reliability IPs, a Venn analysis was conducted using both the 118 IPs obtained from human villus tissue and the 183 IPs from Nicolas et al.'s Co-IP dataset [16]. Seven common IPs were identified, including BAG2, CDK4, CCND1, CDK2, RPS19, RPS10, and STK40 (Fig. 1C). Following literature research, STK40 is a serine/threonine protein kinase. Considering the enrichment of the serine/threonine process in the P57 IPs, STK40 was selected as a potential interaction target for further investigation. The online tool GRAMM-X was used to perform molecular docking on P57 and STK40, confirming a direct interaction between the two proteins (Supplementary Table S2). The docking results displayed the calculated free energy of rigid docking between the proteins as -19.3 kcal/mol, suggesting a close binding between them (Fig. 1D). Furthermore, P57 was precipitated by Co-IP in human villus tissue and HEK-293T cells, the WB results showed that STK40 had a protein interaction with P57 (Fig. 1E).

2. Down-regulation of STK40 expression during CTB fusion

The expression pattern of STK40 was investigated in two distinct VCT fusion models and human villi from early pregnancy. PHT was isolated from human normal

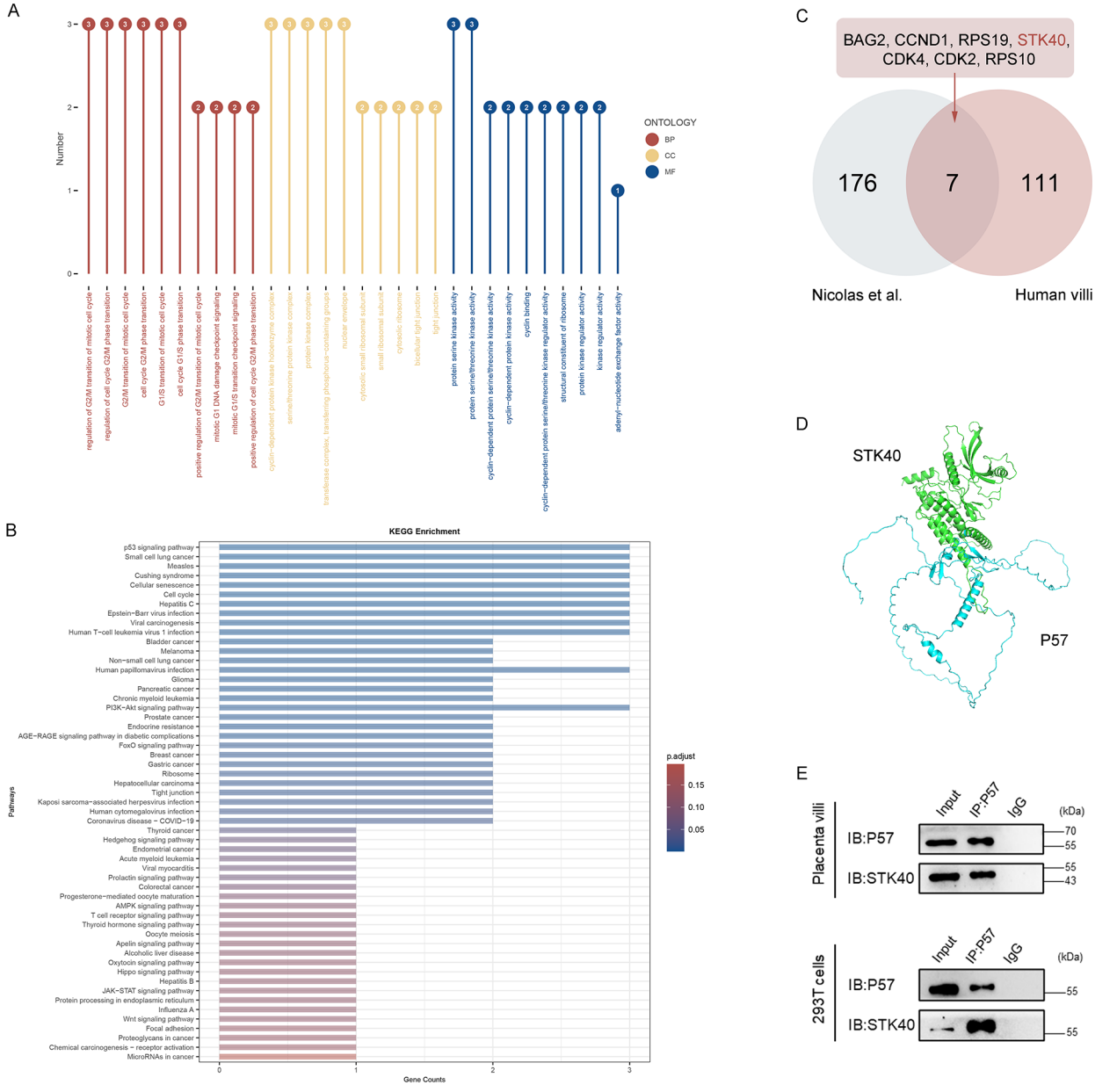

Fig. 1 STK40 interacts with P57. (**A**) GO cluster analysis of P57-interacting proteins (IPs) identified by protein mass spectrometry analysis. The x-axis denotes the GO term, with the number of IPs indicated on the bars. Enrichment levels are shown on the y-axis. GO terms are color-coded: red bars signify Biological Processes (BP), yellow bars represent Cellular Components (CC), and blue bars indicate Molecular Functions (MF). (**B**) KEGG signaling pathway analysis of P57 IPs identified by protein mass spectrometry. (**C**) Venn diagram showcasing the overlap of P57 IPs identified from human villus tissue and Nicolas et al.. (**D**) Visualization of rigid molecular simulation of docking between P57 and STK40. P57 is illustrated in blue, and STK40 is represented in green. (**E**) Co-IP validation of protein interaction between P57 and STK40 in human placental villus tissue and HEK-293T cells. IB, Immunoblotting; Input, protein lysis buffer; IP, immunoprecipitation; IgG, negative control

term placenta, with their purity confirmed by IF staining for CK7 and Vimentin, showing purity levels exceeding 95% (Fig. 2A). VCT were collected after PHT were cultured in vitro for three hours, while spontaneously fused SCT were collected after 48 h. IF staining of E-cadherin (E-CAD) marked the membrane boundary of PHT fusion. Results revealed primary SCT nuclear aggregation, E-CAD disappearance, and down-regulation of STK40 following spontaneous fusion of PHT (Fig. 2B). WB detection of STK40, E-CAD, and CGβ in PHT demonstrated its down-regulation after cell fusion (Fig. 2C). The expression pattern of STK40 in the BeWo cell fusion model induced by the cAMP stimulator, FSK, was consistent with PHT fusion model, indicating down-regulation

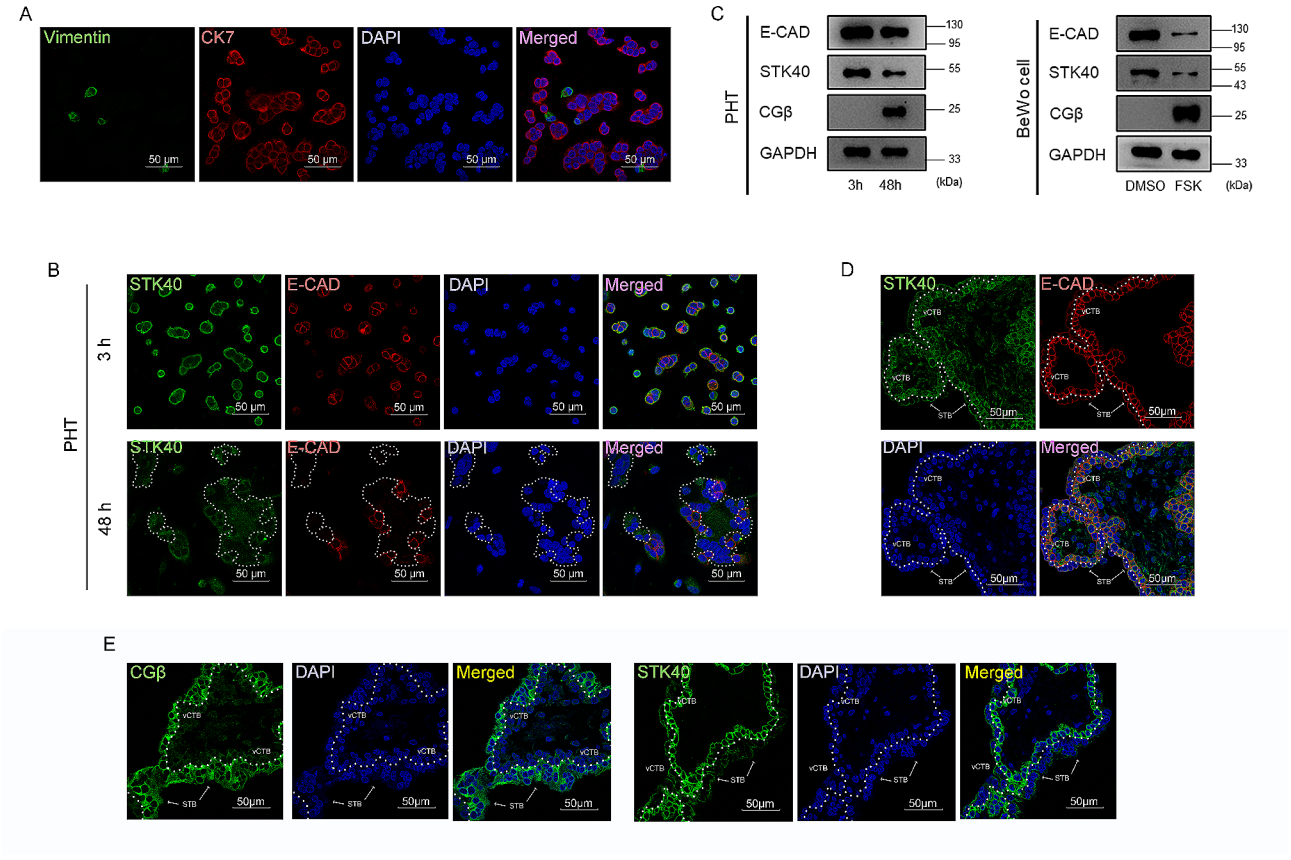

Fig. 2 Expression pattern of STK40 during trophoblast fusion. (**A**) Cell immunofluorescence detection of PHT purity. CK7 labels trophoblast, Vimentin labels stromal cells, DAPI stains nuclear; Scale: 50 μm. (**B**) Cell immunofluorescence detection of STK40 expression pattern in the spontaneous fusion model of PHT. E-CAD labels cell membranes, DAPI stains nuclear; Scale: 50 μm. (**C**) Western blot analysis of STK40, E-CAD, and CGβ protein expression patterns in PHT and BeWo cells. 3 h, primary VCT; 48 h, primary SCT; DMSO, solvent control; FSK, cell fusion inducer. (**D**) Immunofluorescence staining of STK40 expression localization in human villi from 6–8 weeks of gestation age. CK7 labels cytotrophoblasts, DAPI stains nuclear. Scale: 50 μm. (**E**) Immunofluorescence staining of sequential sections showing STK40 and CGβ expression in human villi from 6–8 weeks of gestation age. CGβ labels the syncytiotrophoblast, DAPI stains nuclear. Scale: 50 μm

during cell fusion (Fig. 2C). IF staining of villi at gestational age 6–8 weeks showed that STK40 was highly expressed in the CK7-positive VCT cell layer, and significantly down-regulated in the CK7-negative outer SCT layer (Fig. 2D).

3. Overexpression of STK40 inhibited VCT fusion

Despite STK40 being observed down-regulated during VCT fusion, whether it is critical for the process remains unknown. To explore this issue, STK40 was overexpressed in BeWo cell lines. The CCK8 analysis demonstrated a significant enhancement in the viability of stable STK40-overexpressing (STK40-OE) BeWo cells (Fig. 3A). Furthermore, the EdU experiment confirmed an increased proliferation ability of BeWo cells following STK40 overexpression (Fig. 3B). In the BeWo fusion model induced by FSK, the fluorescence intensity of STK40 decreased with cell fusion, while stable overexpression of STK40 significantly inhibited the fusion process (Fig. 3C). Subsequent WB results revealed that stable overexpression of STK40 not only inhibited the degradation of E-CAD but also suppressed the high secretion of CGβ during FSK-induced VCT fusion (Fig. 3D). Therefore, overexpression of STK40 was found to inhibit VCT fusion.

4. Knockdown of STK40 promoted VCT fusion

Additionally, STK40 was knockdowned in the BeWo cell line, and the CCK8 experiment revealed a decrease in the viability of BeWo cells following the knockdown of STK40 (Fig. 4A). EdU experiments further confirmed that knockdown of STK40 downregulated the proliferative capacity of BeWo cells (Fig. 4B). IF staining results indicated that knockdown of STK40 promoted SCT formation (Fig. 4C); meanwhile, the knockdown of STK40 led to the promotion of the down-regulation of E-CAD expression and the secretion of CGβ during VCT fusion (Fig. 4D), suggesting that knockdown of STK40 facilitated VCT fusion.

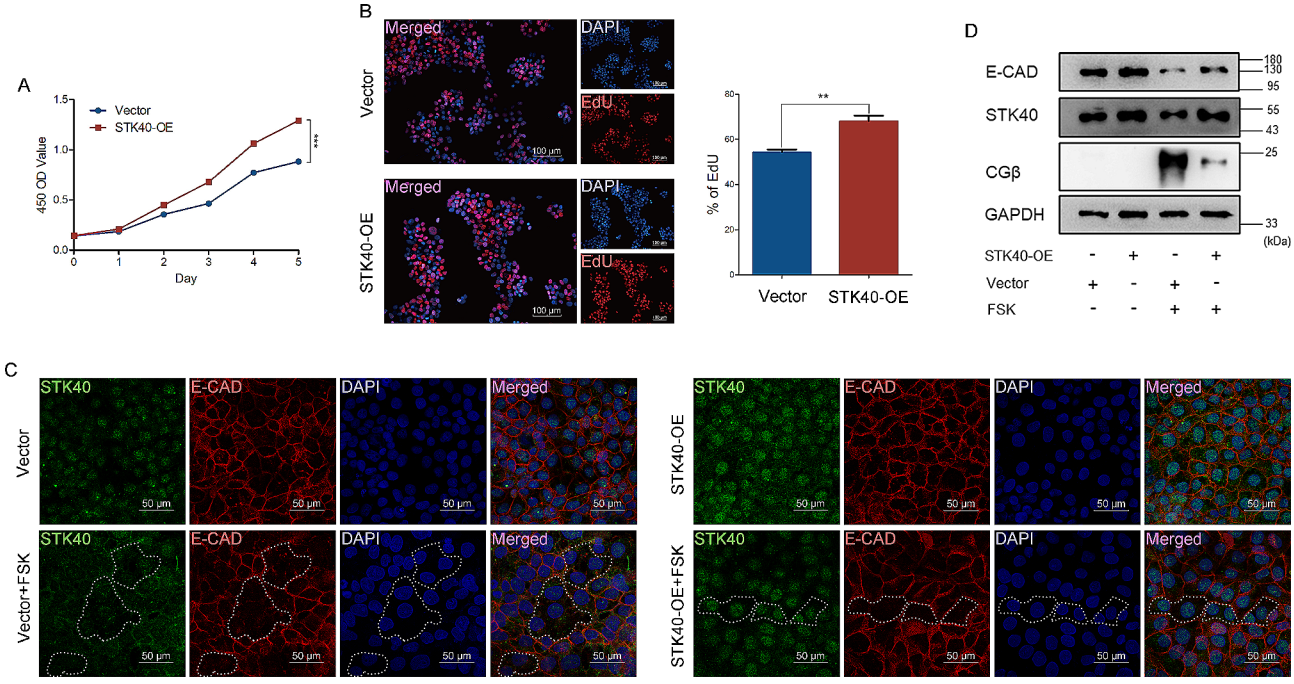

Fig. 3 Overexpression of STK40 inhibited VCT fusion. (**A**) The cell viability of BeWo cells for days 1, 2, 3, 4, and 5 in Vector and STK40-OE groups detected by CCK8. (**B**) EdU assay assesses the number of EdU-positive cells in BeWo cells with Vector and STK40-OE groups. (**C**) Cell immunofluorescence detection of BeWo cells fusion with or without FSK induction in Vector and STK40-OE groups. E-CAD labels cell membranes. Scale: 50 μm. (**D**) Western blot analysis of STK40, E-CAD, and CGβ expression in BeWo cells with or without 48 h FSK induction in Vector and STK40-OE groups. GAPDH was used as a loading control. Vector, empty vector; STK40-OE, STK40 overexpression. ** $P < 0.01$, *** $P < 0.001$

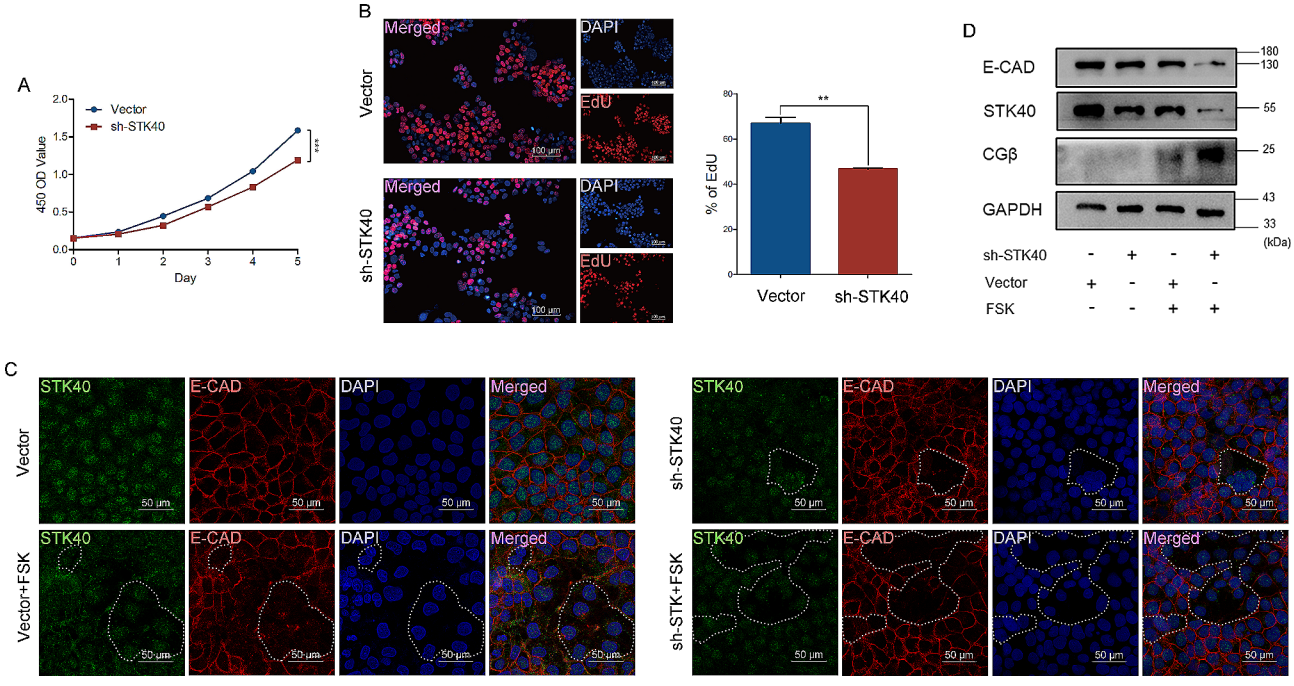

Fig. 4 Knockdown of STK40 promoted VCT fusion. (**A**) The cell viability of BeWo cells for days 1, 2, 3, 4, and 5 in Vector and sh-STK40 groups detected by CCK8. (**B**) EdU assay assesses the number of EdU-positive cells in BeWo cells with Vector and sh-STK40 groups. (**C**) Cell immunofluorescence detection of BeWo cells fusion with or without FSK induction in Vector and sh-STK40 groups. E-CAD labels cell membranes. Scale: 50 μm. (**D**) Western blot analysis of STK40, E-CAD, and CGβ expression in BeWo cells with or without 48 h FSK induction in Vector and sh-STK40 groups. GAPDH was used as a loading control. Vector, empty vector; sh-STK40, knockdown of STK40. ** $P < 0.01$, *** $P < 0.001$

5. STK40 may be involved in cell cycle regulation by binding to the CDK-binding and the Cyclin-binding domain of P57

To further determine the interaction site between STK40 and P57, various truncated mutations of P57 were constructed according to the domain division of P57 (Fig. 5A and B). Regrettably, we encountered difficulties in successfully constructing expressible truncated fragments, particularly within the 142-316 region of P57, owing to its remarkably high GC content, reaching 79% (Fig. 5C) Truncated fragment vectors of P57 and STK40 vector were separately co-transfected into HEK-293T cells. Co-IP analysis revealed that the STK40 interaction domain in P57 was localized to the region between amino acids 1 and 141 in the P57 polypeptide. This region corresponds to both the CDK-binding domain and the Cyclin-binding domain (Fig. 5D). Consequently, it was speculated that STK40 might engage in cell cycle regulation by binding to P57. Flow cytometry was employed to evaluate the impact of STK40 on cell cycle progression. The results showed that overexpression of STK40 led to the arrest of BeWo cells in the S phase; while interfering with STK40 led to arrest of BeWo cells in the G0/G1 phase (Fig. 5E and F).

6. Ubiquitin degradation of P57 by COP1 mediated by STK40

Overexpressing STK40 significantly reduced the levels of P57 protein in BeWo cells. Conversely, knocking down STK40 increased the expression of P57 in BeWo cells (Fig. 6A and B). Intriguingly, these alterations in P57 protein levels did not affect the mRNA levels of P57 (Fig. 6C and D). As per existing literature, COP1, a downstream target factor of STK40, acts as an E3 ubiquitin ligase, facilitating the ubiquitination degradation of STK40 by binding to downstream factors. Thus, we speculated that STK40 might mediate the ubiquitin degradation of P57 by COP1. Co-IP performed in HEK-293T cells demonstrated interactions between P57, STK40, and COP1 (Fig. 6E). To investigate the effect of STK40 on P57 ubiquitination, HA-UB, HA-STK40, P57, and COP1 plasmids were transfected into HEK-293T cells, either separately

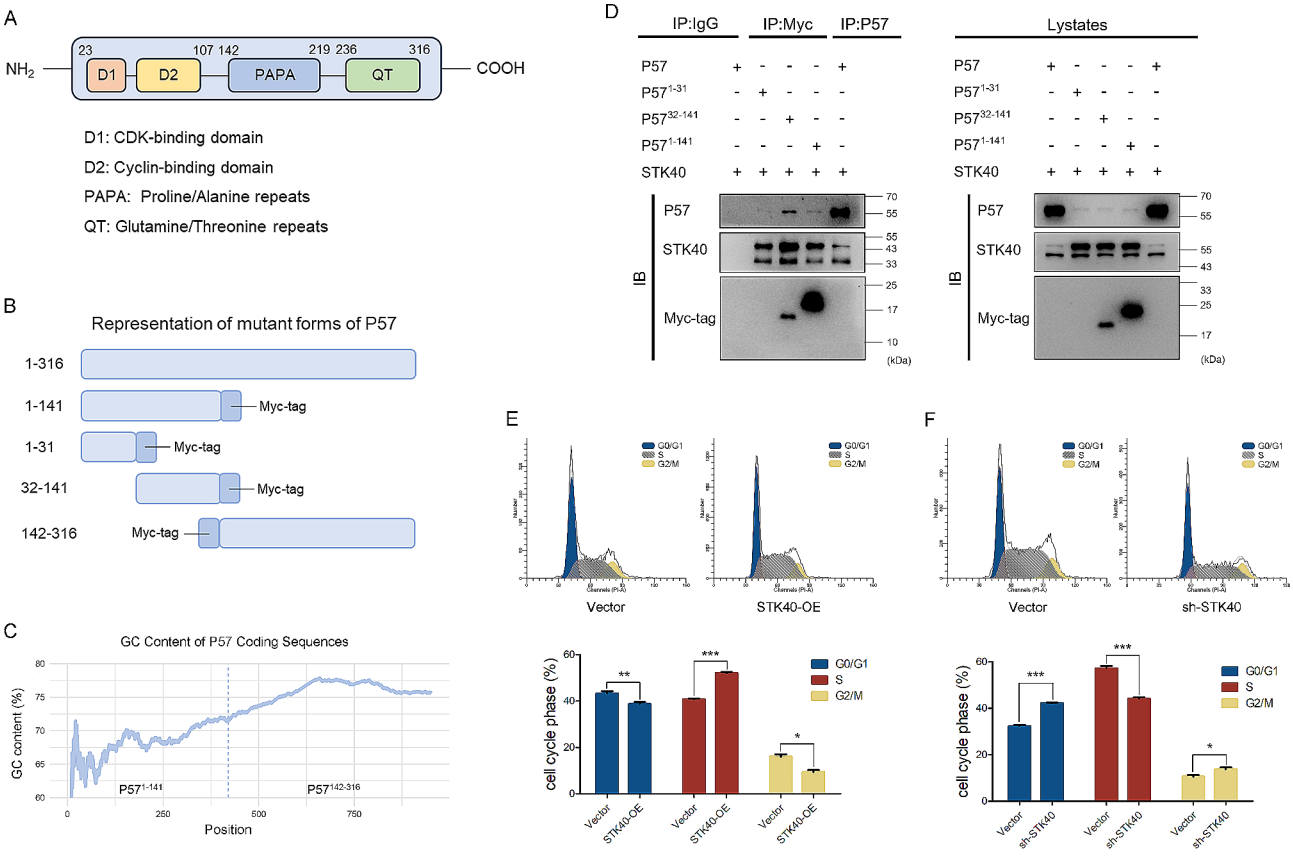

Fig. 5 Search for STK40 interaction site with by P57 truncation mutation strategy. (**A**) A schematic diagram of P57 domain, depicting the CDK-binding domain, Cyclin-binding domain, Proline-rich region (PAPA), proline-alanine repeats (QT), PCNA-binding region, and Skp2-dependent degradation domain. (**B**) Schematic diagram illustrating the construction of Myc-P57 truncation mutants. (**C**) Line chart displaying the GC content within the coding sequence of P57. (**D**) Co-IP validation of the interaction between STK40 and truncated mutants of P57 in HEK-293T cells. IB, Immunoblotting; Lystates: protein lysis buffer; IP: immunoprecipitation; IgG: negative control. (**E**) Flow cytometry analysis of cell cycle progression in BeWo cells with Vector and STK40-OE groups. (**F**) Flow cytometry analysis of cell cycle progression in BeWo cells with Vector and sh-STK40 groups. * $P < 0.05$, ** $P < 0.01$

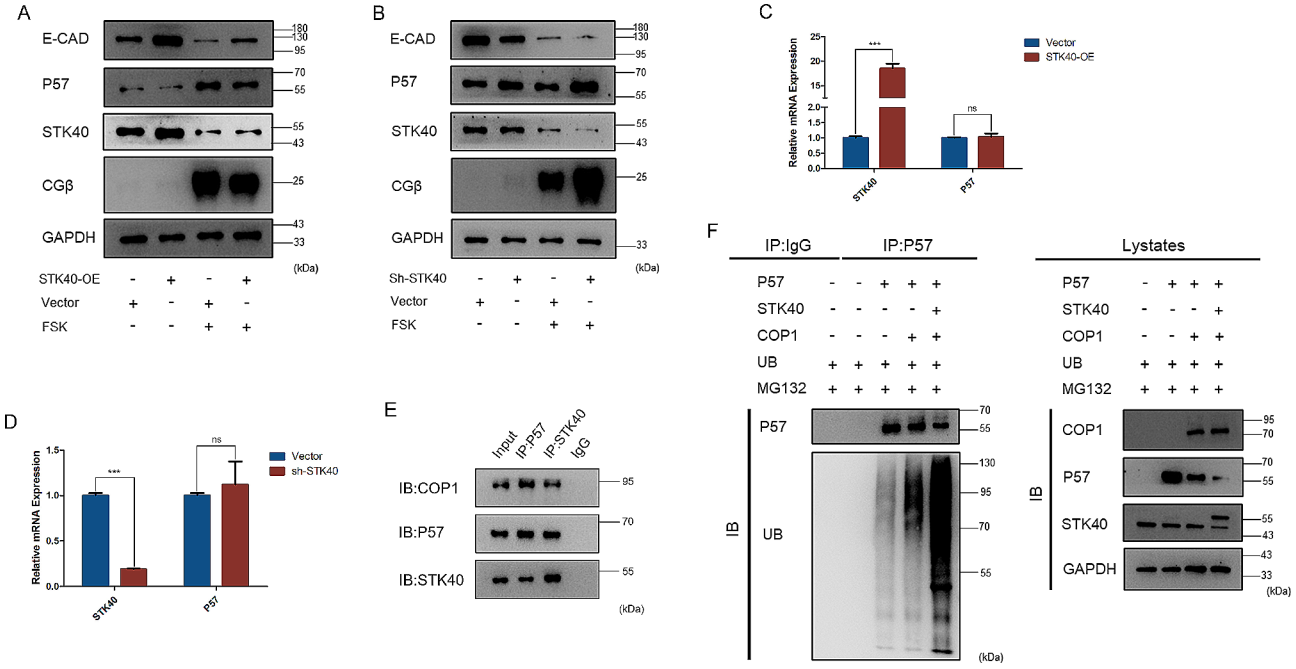

Fig. 6 STK40 promoted ubiquitination degradation of P57 through COP1. (**A**) Western blot analysis of STK40, E-CAD, CGβ, and P57 in BeWo cells with or without 72 h FSK induction in Vector and STK40-OE groups. GAPDH was used as a loading control. (**B**) Western blot analysis of STK40, E-CAD, CGβ, and P57 in BeWo cells with or without 72 h FSK induction in Vector and sh-STK40 groups. GAPDH was used as a loading control. (**C**) RT-qPCR was utilized to measure the mRNA expression of STK40 and P57 in BeWo cells in Vector and STK40-OE groups. (**D**) RT-qPCR was utilized to measure the mRNA expression of STK40 and P57 in BeWo cells in Vector and sh-STK40 groups. (**E**) Co-IP was performed to validate the protein-protein interactions between P57, COP1, and HA-STK40 in HEK-293T cells. (**F**) Western blot analysis was conducted to detect the ubiquitination levels of P57. ns, no statistical significance; *** $P < 0.001$

or together. Subsequently, cells were treated with the proteasome inhibitor MG132 before harvesting for Co-IP. The results demonstrate that the introduction of COP1 leads to an increase in the ubiquitination level of P57, and overexpression of STK40 further enhances the ubiquitination of P57 (Fig. 6F). These findings suggest that STK40 promotes the ubiquitination and degradation of P57 through COP1.

7. Transcriptome analysis provides evidence that STK40 ubiquitinates P57

RNA-seq analysis was performed on control BeWo cells, stably overexpressing STK40, and knockdown of STK40. DEGs between STK40 overexpression cells and control cells were identified (Supplementary Table S3), including 336 up-regulated genes and 736 down-regulated genes (absolute fold change > 0.5, $P < 0.05$; Fig. 7A). Moreover, 703 up-DEGs and 367 down-DEGs were detected between the knockdown of STK40 group and the control group (absolute fold change > 0.5, $P < 0.05$; Fig. 7B). The overlap between up-regulated DEGs after STK40 overexpression and down-regulated DEGs after knockdown of STK40, and the overlap of down-regulated DEGs after STK40 overexpression with up-regulated DEGs after knockdown of STK40, suggested potential downstream targets of STK40 (Fig. 7C and D). These targets included genes associated with P57 (e.g., RB1 and TERT), the E3 ubiquitin-protein ligase complex (including KLHL24, RNF13, RNF43, FBXO30, FBXO32, and SPOPL), and SCT marker genes (e.g., GH2, CGA, CSH1, CSH2, PSG3, and PSG5). GO analysis of these potential downstream targets highlighted enrichment in BP related to endoplasmic reticulum stress response and ubiquitin-dependent endoplasmic reticulum-associated degradation (ERAD). Enriched CC pathway included endoplasmic reticulum containing protein complexes and melanosomes, while the MF pathways involved folding chaperone binding and isomerase activity (Fig. 7E). Further KEGG analysis showed that the common DEGs enriched in the endoplasmic reticulum, cytokine-cytokine receptor interaction, and JAK-STAT signaling path (Fig. 7F). The above results also provide possible evidence for ubiquitination degradation of P57 by STK40.

8. Abnormally high expression of STK40 in PE placenta

Previous studies have confirmed that in the placenta of patients with PE, there is a disruption in the balance of trophoblast proliferation and differentiation, manifesting as decreased cell syncytialization, increased apoptosis, and necrosis of trophoblast layer cells [2]. The expression of STK40 in PE placenta was confirmed using RNA-seq data (GSE149812) from the Gene Expression Omnibus (GEO) database. Results indicated a significant up-regulation of STK40 expression in the placentas of women

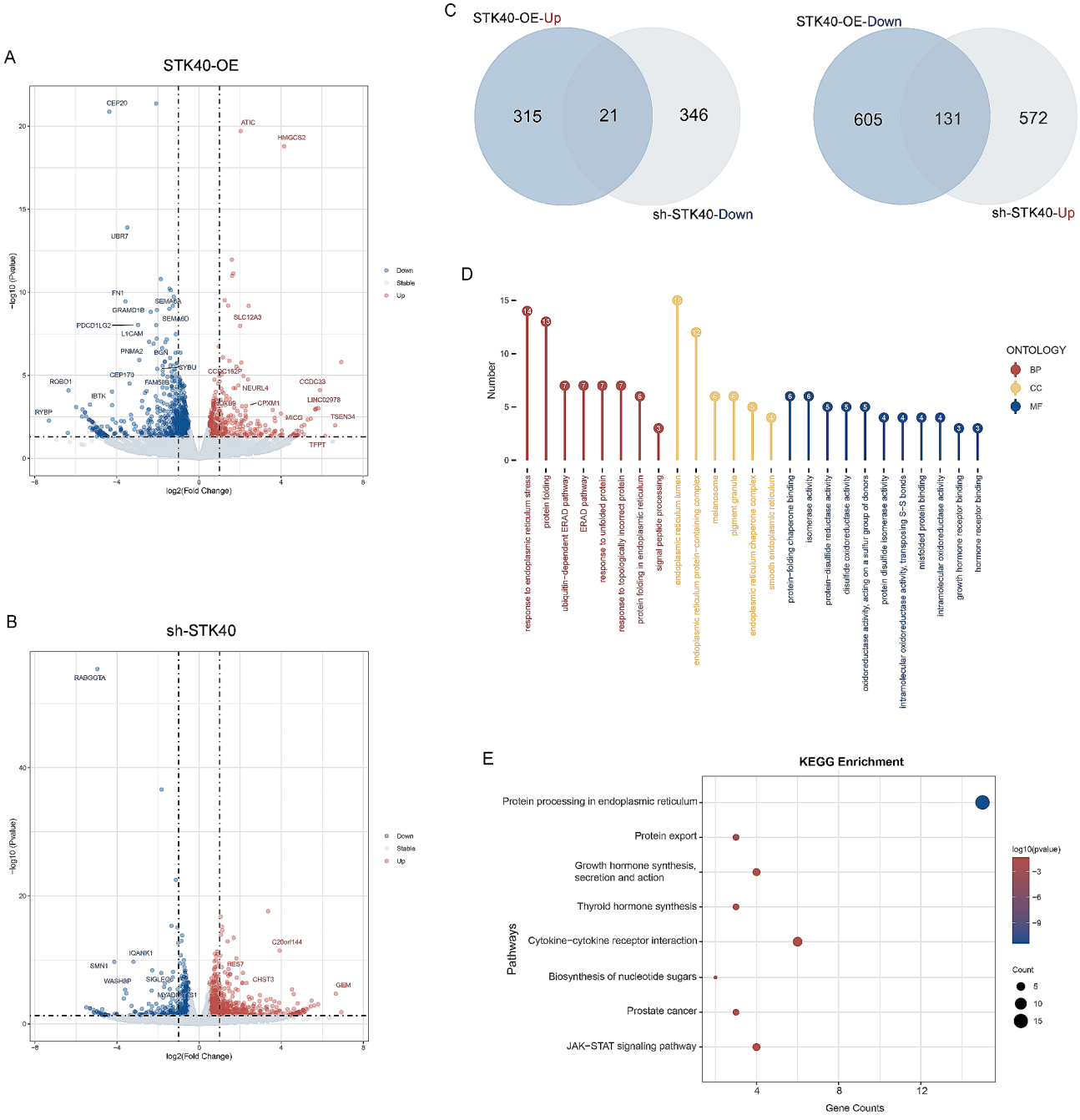

Fig. 7 Transcriptome shows potential downstream targets of STK40. (**A**) Volcano maps illustrating DEGs in Vector and STK40-OE groups. Red points indicate up-regulation DEGs, blue indicates down-regulation DEGs, and the gray point represents non-significant DEGs. (**B**) Volcano maps showcasing DEGs in Vector and sh-STK40 groups. (**C**) Venn diagram displaying the overlap between up-regulated DEGs after STK40 overexpression and down-regulated DEGs after knockdown of STK40. And the Venn diagram of the down-regulated DEGs after STK40 overexpression and the up-regulated DEGs after knockdown of STK40. (**D**) GO analysis of the potential downstream targets of STK40. (**E**) KEGG pathway enrichment analysis of potential downstream targets of STK40

with PE (Fig. 8A). Further confirmation by IF staining and WB demonstrated abnormal up-regulation of STK40 expression in PE placenta compared to normal full-term placenta (Fig. 8B and C).

Discussion

The prerequisite for VCT fusion into SCT involves the withdrawal of VCT from the mitotic cycle to the G0 phase [5]. However, the cell cycle regulatory mechanisms that control trophoblast proliferation and initiate trophoblast fusion have not been fully characterized. The

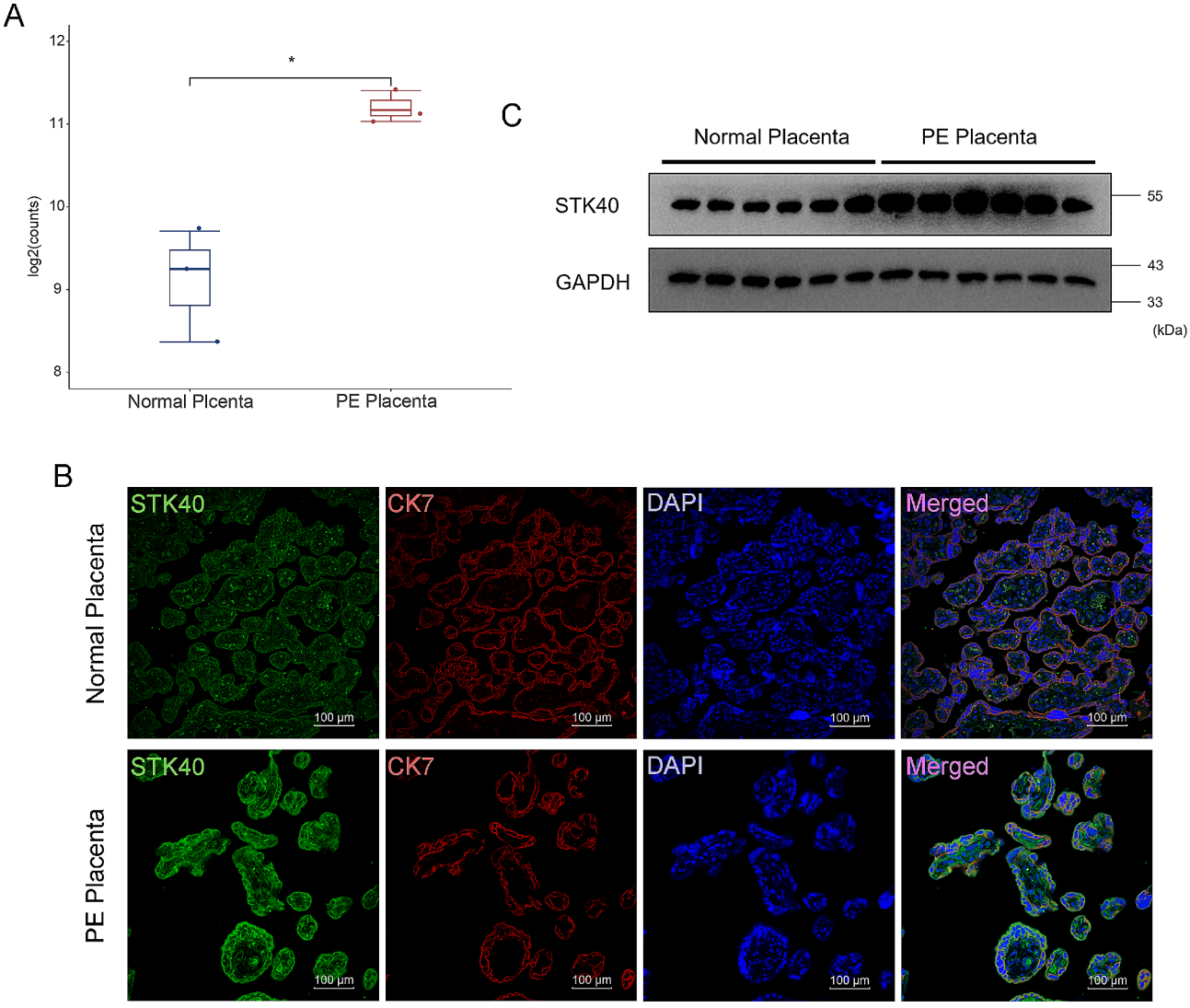

Fig. 8 Abnormally high expression of STK40 in PE placenta. (**A**) Expression levels of STK40 in normal placenta and PE placenta from the GSE149812 dataset. (**B**) Immunofluorescence detection of STK40 in normal placenta and PE placenta. CK7 labels cytotrophoblasts, DAPI stains nuclear; Scale: 50 μm. (**C**) Western blot analysis of STK40 in normal placenta and PE placenta

imprinted gene P57 has been identified as a pivotal factor in mediating cell cycle exit and instigating cell fusion in trophoblast cells. P57 is notably expressed at high levels in intermediate VCT with fusion capability [11]. Notably, aberrantly high P57 expression can lead to trophoblast hyperproliferation, potentially causing hydatidiform mole [17–19]. Conversely, abnormally low P57 expression significantly decreases intermediate VCT, potentially contributing to conditions like PE [13, 14, 20]. Thus, exploring the precise regulatory mechanisms governing P57 expression timing and levels is of paramount importance in resolving trophoblast fusion complications.

In this study, STK40 was identified as a new interacting protein of P57 through various methods. STK40, characterized as a serine/threonine pseudokinase, lacks conserved amino acid residues within its kinase structural domain required for ATP binding. STK40 exhibits diverse roles in different tissues or organs. For instance, knockout of STK40 in mice resulted in multiple organ failure and perinatal death. Subsequent investigations revealed that STK40 deficiency caused c-JUN protein accumulation, suppressed WNT signaling activity, and impeded mesodermal differentiation in mouse embryos [21]. High STK40 expression promoted myoblast differentiation by maintaining the transcriptional activity of myocyte enhancer factor 2 (MEF2) [22]. Conversely, knockdown of STK40 resulted in increased protein levels of C/EBP protein, promoting adipocyte differentiation in mouse embryonic fibroblasts and MSCs [23]. However, the role of STK40 in trophoblast cells remains unreported. Here, we discovered that STK40 was downregulated during trophoblast fusion. Despite not affecting

the transcriptional level of P57, knockdown of STK40 resulted in elevated P57 protein levels in BeWo cells, stimulating trophoblast differentiation and potentially influencing cell cycle regulation. Hence, STK40 may play a role in cell differentiation through multiple pathways within trophoblast cells.

As a member of the pseudokinase family, STK40 lacks the protein kinase activity required for phosphorylating substrates but retains the capability to interact with signaling proteins. It has been established that STK40 interacts with the COP1 WD40 domain of the E3 ubiquitin ligase [24]. The COP1 WD40 domain is responsible for recognizing substrates and tagging them for ubiquitination [25]. Previous studies have demonstrated that COP1 could ubiquitinate modify and degrade P53 and P27, which is a member of the KIP/CIP family with P57, and thus is involved in proliferation and cell cycle regulation in a variety of cells [26–29]. Here, we revealed that COP1 ubiquitinated P57 and that overexpression of STK40 enhanced the ubiquitination of P57 by COP1. Additionally, our transcriptome sequencing analysis of STK40 overexpression and knockdown of STK40 in BeWo cells revealed that the downstream target genes of STK40 were enriched in the ubiquitin-dependent ERAD pathway. This finding supports the possibility that STK40 might recruit the ubiquitin ligase complex to downregulate P57. Previously, our research indicated that P57 can drive trophoblast fusion [11], but it is noteworthy that P57 is only present in intermediate VCT. P57 is up-regulated for expression during trophoblast fusion and is down-regulated for expression/non-expression in definitive SCT. If P57 is consistently expressed in high amounts in SCT it promotes SCT apoptosis. Thus, STK40 mediating the degradation of P57 by COP1 in the present study provided a possible explanation for the homeostatic regulation of P57 protein during trophoblast fusion. Studies highlighted that PE placental VCT fusion is severely deficient, which may result from the inability to drive VCT to exit the mitotic cell cycle to initiate fusion due to aberrant P57 expression [2, 13]. Our discovery of abnormally high STK40 expression in PE partially explains the abnormal expression of P57 in PE placentas. Future investigations should consider employing primary trophoblast cells and trophoblast stem cell lines whenever possible to reinforce the conclusions drawn in this study.

Conclusions

This study demonstrated that STK40 is a key regulator of human placental trophoblast fusion, revealing an important role for STK40 in regulating P57 protein homeostasis.

Supplementary Information

The online version contains supplementary material available at https://doi.org/10.1186/s12967-024-05360-y.

Supplementary Material 1

Supplementary Material 2

Supplementary Material 3

Supplementary Material 4

Acknowledgements

We would like to thank the donors and the obstetrical staff of The First Affiliated Hospital of Chongqing Medical University Department of Obstetric for placental specimens.

Author contributions

X.Li. and T-H.Liu. designed the study. Y-X.Wang., Y-B.Ding., T-H.Liu. contributed reagents. X.Luo and X-M.Chen contributed sample. L-Z.Shao., Y-H.Wang. and J.Sheng performed bioinformatics analysis of the RNA-seq data. X.Li., Z-H.Li., Q-Y.Cai., S.Wang. and H.Chen. performed the experiments and data analysis and interpretation. X.Li., Z.Shao. and T-H.Liu. wrote the manuscript.

Funding

This work was funded by the National Natural Science Foundation of China (81801458 and 82271707), Program for Youth Innovation in Future Medicine, Chongqing Medical University (W0068), and the National College Students Innovation and Entrepreneurship Training Program (202110631002 and 202210631005).

Data availability

The data underlying this article will be shared on reasonable request corresponding author.

Declarations

Ethics approval and consent to participate

The Human Research Ethics Board of the Chongqing Medical University approved the human placental tissues collection procedures (#2022127).

Consent for publication

Not applicable.

Competing interests

The authors declare no competing interests.

Author details

[1]Department of Bioinformatics, School of Basic Medical Sciences, Chongqing Medical University, Chongqing 400016, China
[2]The Joint International Research Laboratory of Reproduction and Development, Chongqing Medical University, Box 197, No.1 Yixueyuan Rd, Chongqing 400016, China
[3]Medical Laboratory Department, Traditional Chinese Medicine Hospital of Yaan, Sichuan 625099, China
[4]Department of Obstetrics, The First Affiliated Hospital of Chongqing Medical University, Chongqing 400016, PR China

Received: 6 February 2024 / Accepted: 29 May 2024
Published online: 20 September 2024

References

1. Io S, Kondoh E, Chigusa Y, Kawasaki K, Mandai M, Yamada AS. New era of trophoblast research: integrating morphological and molecular approaches. Hum Reprod Update. 2020;26:611–33.
2. Redman CWG, Staff AC, Roberts JM. Syncytiotrophoblast stress in preeclampsia: the convergence point for multiple pathways. Am J Obstet Gynecol. 2022;226:S907–27.

3. Burton GJ, Redman CW, Roberts JM, Moffett A. Pre-eclampsia: pathophysiology and clinical implications. BMJ. 2019;366:l2381.
4. Renaud SJ, Jeyarajah MJ. How trophoblasts fuse: an in-depth look into placental syncytiotrophoblast formation. Cell Mol Life Sci CMLS. 2022;79:433.
5. Liu Y, Fan X, Wang R, Lu X, Dang Y-L, Wang H, et al. Single-cell RNA-seq reveals the diversity of trophoblast subtypes and patterns of differentiation in the human placenta. Cell Res. 2018;28:819–32.
6. Lu X, Wang R, Zhu C, Wang H, Lin H-Y, Gu Y, et al. Fine-tuned and cell-cycle-restricted expression of Fusogenic protein Syncytin-2 maintains functional placental syncytia. Cell Rep. 2017;21:1150–9.
7. Meinhardt G, Haider S, Kunihs V, Saleh L, Pollheimer J, Fiala C, et al. Pivotal role of the transcriptional co-activator YAP in trophoblast stemness of the developing human placenta. Proc Natl Acad Sci U S A. 2020;117:13562–70.
8. Creff J, Besson A. Functional versatility of the CDK inhibitor p57Kip2. Front Cell Dev Biol. 2020;8:584590.
9. Xing D, Miller K, Beierl K, Ronnett BM. Loss of p57 expression in Conceptions Other Than Complete Hydatidiform Mole: a Case Series with emphasis on the etiology, Genetics, and clinical significance. Am J Surg Pathol. 2022;46:18–32.
10. Takahashi S, Okae H, Kobayashi N, Kitamura A, Kumada K, Yaegashi N, et al. Loss of p57KIP2 expression confers resistance to contact inhibition in human androgenetic trophoblast stem cells. Proc Natl Acad Sci U S A. 2019;116:26606–13.
11. Song H-L, Liu T-H, Wang Y-H, Li F-F, Ruan L-L, Adu-Gyamfi EA, et al. Appropriate expression of P57kip2 drives trophoblast fusion via cell cycle arrest. Reprod Camb Engl. 2021;161:633–44.
12. Takahashi K, Yoneyama Y, Koizumi N, Utoguchi N, Kanayama N, Higashi N. Expression of p57KIP2 reduces growth and invasion, and induces syncytialization in a human placental choriocarcinoma cell line, BeWo. Placenta. 2021;104:168–78.
13. Kanayama N, Takahashi K, Matsuura T, Sugimura M, Kobayashi T, Moniwa N, et al. Deficiency in p57Kip2 expression induces preeclampsia-like symptoms in mice. Mol Hum Reprod. 2002;8:1129–35.
14. Kreis N-N, Friemel A, Jennewein L, Hoock SC, Hentrich AE, Nowak T, et al. Functional analysis of p21Cip1/CDKN1A and its family members in trophoblastic cells of the Placenta and its roles in Preeclampsia. Cells. 2021;10:2214.
15. Gestational Hypertension and Preeclampsia. ACOG Practice Bulletin, Number 222. Obstet Gynecol. 2020;135:e237–60.
16. Duquesnes N, Callot C, Jeannot P, Daburon V, Nakayama KI, Manenti S, et al. p57(Kip2) knock-in mouse reveals CDK-independent contribution in the development of Beckwith-Wiedemann syndrome. J Pathol. 2016;239:250–61.
17. Popiolek DA, Yee H, Mittal K, Chiriboga L, Prinz MK, Caragine TA, et al. Multiplex short tandem repeat DNA analysis confirms the accuracy of p57(KIP2) immunostaining in the diagnosis of complete hydatidiform mole. Hum Pathol. 2006;37:1426–34.
18. Gaillot-Durand L, Patrier S, Aziza J, Devisme L, Riera A-C, Marcorelles P, et al. p57-discordant villi in hydropic products of conception: a clinicopathological study of 70 cases. Hum Pathol. 2020;101:18–30.
19. Zhao Y, Huang B, Zhou L, Cai L, Qian J. Challenges in diagnosing hydatidiform moles: a review of promising molecular biomarkers. Expert Rev Mol Diagn. 2022;22:783–96.
20. Knox KS, Baker JC. Genome-wide expression profiling of placentas in the p57Kip2 model of pre-eclampsia. Mol Hum Reprod. 2007;13:251–63.
21. Hu J, Li S, Sun X, Fang Z, Wang L, Xiao F, et al. Stk40 deletion elevates c-JUN protein level and impairs mesoderm differentiation. J Biol Chem. 2019;294:9959–72.
22. He K, Hu J, Yu H, Wang L, Tang F, Gu J, et al. Serine/Threonine kinase 40 (Stk40) functions as a Novel Regulator of skeletal muscle differentiation. J Biol Chem. 2017;292:351–60.
23. Yu H, He K, Wang L, Hu J, Gu J, Zhou C, et al. Stk40 represses adipogenesis through translational control of CCAAT/enhancer-binding proteins. J Cell Sci. 2015;128:2881–90.
24. Durzynska I, Xu X, Adelmant G, Ficarro SB, Marto JA, Sliz P et al. STK40 Is a Pseudokinase that Binds the E3 Ubiquitin Ligase COP1. Struct Lond Engl. 1993. 2017;25:287–94.
25. Uljon S, Xu X, Durzynska I, Stein S, Adelmant G, Marto JA et al. Structural Basis for Substrate Selectivity of the E3 Ligase COP1. Struct Lond Engl. 1993. 2016;24:687–96.
26. Heishima K, Mori T, Sakai H, Sugito N, Murakami M, Yamada N, et al. MicroRNA-214 promotes apoptosis in Canine Hemangiosarcoma by targeting the COP1-p53 Axis. PLoS ONE. 2015;10:e0137361.
27. Choi HH, Guma S, Fang L, Phan L, Ivan C, Baggerly K, et al. Regulating the stability and localization of CDK inhibitor p27(Kip1) via CSN6-COP1 axis. Cell Cycle Georget Tex. 2015;14:2265–73.
28. Gu C, Lu T, Wang W, Shao M, Wei R, Guo M, et al. RFWD2 induces cellular proliferation and selective proteasome inhibitor resistance by mediating P27 ubiquitination in multiple myeloma. Leukemia. 2021;35:1803–7.
29. Liu J, Zhang C, Wang X, Hu W, Feng Z. Tumor suppressor p53 cross-talks with TRIM family proteins. Genes Dis. 2021;8:463–74.

Publisher's Note